Inorganic Chemistry
Article

Biomimetic Oxidation of 3,5-Di-*tert*-butylcatechol by Dioxygen via Mn-Enhanced Base Catalysis

Imola Cs. Szigyártó,*,† **László I. Simándi,***,† **László Párkányi,‡ László Korecz,‡ and Gitta Schlosser‡**

Chemical Research Center, Institute of Surface Science and Catalysis, and Institute of Structural Research, Hungarian Academy of Sciences, P.O. Box 17, H-1525 Budapest, Hungary

The 6-coordinate dioximatomanganese(II) complex $[Mn(HL)(CH_3OH)]^+$ (**2**, where H_2L is $[HON{=}C(CH_3)C(CH_3){=}NCH_2{-}CH_2]_2NH$), formed by instant solvolysis of $[Mn_2(HL)_2](BPh_4)_2$ (**1**) in methanol, accelerates the triethylamine (TEA)-catalyzed oxidation of 3,5-di-*tert*-butylcatechol (H_2dtbc) by O_2 to the corresponding *o*-benzoquinone. Significantly, **2** alone has no catalytic effect. The observed rate increase can be explained by the interaction of **2** with the hydroperoxo intermediate $HdtbcO_2^-$ formed from $Hdtbc^-$ and O_2 in the TEA-catalyzed oxidation. The kinetics of the TEA-catalyzed and Mn-enhanced reaction has been studied by gas-volumetric monitoring of the amount of O_2 consumed. The initial rate of O_2 uptake (V_{in}) shows a first-order dependence on the concentration of **2** and O_2 and saturation kinetics with respect to both H_2dtbc and TEA. The observed kinetic behavior is consistent with parallel TEA-catalyzed and Mn-enhanced oxidation paths. The 3,5-di-*tert*-butylsemiquinone anion radical is an intermediate detectable by electron spin resonance (ESR) spectroscopy. The dimeric catalyst precursor has been characterized by X-ray diffraction and electrospray ionization mass spectrometry and the monomeric catalyst by ESR spectroscopy.

Introduction

Mn-containing redox enzymes are ubiquitous in nature and perform a number of vital functions.[1] The most notable examples are manganese superoxide dismutase,[2a] manganese catalases,[2b] peroxidase,[2c] and manganese-dependent dioxygenases.[2d] Photosynthetic water oxidation by photosystem II is controlled by a tetramanganese cluster.[2e,f] The modeling approach has been extensively used to elucidate the structure and function of Mn redox enzymes.[3] The reactions of O_2 and its reduced forms with Mn have been reviewed by Pecoraro et al.[4]

Catechol oxidases are plant enzymes containing dinuclear Cu centers, which catalyze the oxidation of catechols to quinones.[5] Catecholases are also involved in the formation of melanin pigments and the enzymatic browning of fruits.[6] Functional catecholase models based on Cu,[7] Fe,[8] Co,[8,9] and Zn[10] have been investigated to shed light on the reaction mechanisms involved and to help design "bioinspired" catalyst systems for various reactions requiring activation of O_2.

The abundance of O_2-activating Co, Cu, and Fe catalysts[11] is in contrast with the relative rarity of Mn complexes capable of that function under homogeneous conditions. Reversible O_2 adducts have been reported and characterized as metal–peroxo species for manganese(II) porphyrin derivatives,[12] a manganese(III) diene complex,[13] and a dinuclear manganese-

* To whom correspondence should be addressed. E-mail: imcsi@chemres.hu (I.Cs.S), simandi@chemres.hu (L.I.S.).
† Chemical Research Center, Institute of Surface Science and Catalysis.
‡ Institute of Structural Research.

(1) Sigel, A.; Sigel, H. Manganese and Its Role in Biological Processes. *Metal Ions in Biological Systems*; Marcel Dekker: New York, 2000; Vol. 37.
(2) (a) Whittaker, J. H. Reference 1; Chapter 18, pp 587−611. (b) Yoder, D. W.; Hwang, J.; Penner-Hahn, J. E. Reference 1; Chapter 16, pp 527−557. (c) Gold, M. H.; Youngs, H. L.; Sollewijn Gelpke, M. D. Reference 1; Chapter 17, pp 559−586. (d) Que, L., Jr.; Reynolds, M. F. Reference 1; Chapter 15, pp 505−525. (e) Hoganson, C. W.; Babcock, G. T. Reference 1; Chapter 19, pp 613−656. (f) Ferreira, K. N.; Iverson, T. M.; Maghlaoui, K.; Barber, J.; Iwata, S. *Science* **2004**, *303*, 1831−1838.
(3) Pecoraro, V. L.; Hsieh, W.-Y. Reference 1; Chapter 14, pp 429−504.

(4) (a) Pecoraro, V. L.; Baldwin, M. J.; Gelasco, A. *Chem. Rev.* **1994**, *94* (3), 807−826. (b) Wu, A. J.; Penner-Hahn, J. E.; Pecoraro, V. L. *Chem. Rev.* **2004**, *104* (2), 903−938.
(5) (a) Solomon, E. I.; Sundaram, U. M.; Machonkin, T. E. *Chem. Rev.* **1996**, *96* (7), 2563−2606. (b) Than, R.; Feldmann, A. A.; Krebs, B. *Coord. Chem. Rev.* **1999**, *182*, 211−241. (c) Gerdemann, C.; Eicken, C.; Krebs, B. *Acc. Chem. Res.* **2002**, *35* (3), 183−191. (d) Zhang, C. X.; Liang, H.-C.; Humphreys, K. J.; Karlin, K. D. In *Advances in Catalytic Activation of Dioxygen by Metal Complexes*; Simándi, L. I., Ed.; Kluwer Academic Publishers: Dordrecht, The Netherlands, 2003; pp 79−121.

(IV) 1,4,7-trimethyl-1,4,7-triazacyclononane.[14] Additional examples of O_2 binding are manganese phthalocyanins,[15] a Mn complex of 3,5-di-*tert*-butylcatecholate,[16] and a series of $[Mn^{II}X_2(PR_3)]$ complexes.[17] Manganese(II) tris[(*R*)-pyrazolyl]borate complexes undergo oxidation with O_2 to the Mn^{III} derivative.[18a] The peroxomanganese(III) complex $[Mn(O_2)(3,5\text{-}^iPr_2pzH)(HB(3,5\text{-}^iPr_2pz)_3)]_2$ was made using H_2O_2[18b] rather than O_2. Mn^{II}(salpr) reacts with O_2, affording the bridged $[Mn^{IV}(salpr)(\mu_2\text{-}O)]_2$ dimer via a Mn^{III} intermediate.[19] $[Mn^{II}(salpn)]$ reacts similarly but is assumed to bypass the Mn^{III} stage.[20] Further Mn^{II} complexes reacting irreversibly with O_2 are those of anionic O-donor ligands in preference over neutral N-donor ligands.[21]

Manganese porphyrins undergo irreversible oxidation upon reaction with O_2 in nondonor solvents. The air oxidation of manganese(II) tetraphenylporphyrin in chlorobenzene yields a monooxo-bridged $Mn^{II,III}$ mixed-valence complex.[22,23]

The kinetics and mechanisms of metal-catalyzed autoxidation reactions, including Mn systems, have been recently reviewed.[24] Aerobic catechol oxidation catalysis has been reported by Funabiki et al. for a bis(μ-oxo)dimanganese-(III,III) complex via a manganese(II) semiquinonato intermediate.[25]

Our earlier work was concerned with the biomimetic catalytic oxidation of 3,5-di-*tert*-butylcatechol (H_2dtbc), using the functional catecholase model bis(dimethylglyoximato)-cobalt(II) and -iron(II) complexes [also known as cobaloxime-(II)[8c,9] and ferroxime(II) derivatives].[8a] Kinetic investigations of these models were carried out to help elucidate the mechanism of the underlying biological catecholase reaction.[8a,c,9b] As an extension of the scope of oximatoiron(II) models beyond ferroximes, some new dioximatoiron complexes with less rigid coordination spheres have been synthesized, which turned out to possess catecholase activity.[8b,c] The general mechanistic pattern typical for these dioximato-metal(II) complexes is the formation of a ternary catalyst–O_2–substrate intermediate, which in the rate-determining step undergoes H-atom transfer, generating a semiquinone anion radical.[7c,d]

In this paper, we report the (a) synthesis and characterization of the dimeric Mn^{II} complex $[Mn_2(HL)_2](BPh_4)_2$ (**1**), where H_2L is $[HON=C(CH_3)C(CH_3)=NCH_2CH_2]_2NH$, and (b) a kinetic study of the remarkable accelerating effect that monomeric $[Mn(HL)(CH_3OH)]^+$ (**2**) exerts on the triethylamine (TEA)-catalyzed (base-catalyzed) oxidation of 3,5-H_2dtbc in MeOH.

Experimental Section

The ligand H_2L was synthesized by the condensation of 2 equiv of diacetylmonoxime with 1 equiv of diethylenetriamine in methanol (MeOH) according to a reported procedure.[26] The product gave satisfactory elemental analyses for $C_{12}H_{23}N_5O_2$. Its purity was checked by ^{1}H NMR spectroscopy.

Electron spin resonance (ESR) spectra were recorded on a Bruker ELEXYS E500 CW-EPR spectrometer in a MeOH solution. The catalytic oxidation of 3,5-di-*tert*-butylcatechol (H_2dbc) was monitored under O_2, keeping the solution saturated with O_2 throughout

(6) (a) Gentschev, P.; Möller; N.; Krebs, B. *Inorg. Chim. Acta* **2000**, *300*, 442–452. (b) Wegner, R.; Gottschaldt, M.; Görls, H.; Jäger, E.-G.; Klemm, D. *Chem.—Eur. J.* **2001**, *7* (10), 2143–2157. (c) Fernandes, C.; Neves, A.; Bortoluzzi, A. J.; Mangrich, A. S.; Rentschler, E.; Szpoganicz, B.; Schwingel, E. *Inorg. Chim. Acta* **2001**, *320*, 12–21. (d) Torelli, S.; Belle, C.; Hamman, S.; Pierre, J. L.; Saint-Aman, E. *Inorg. Chem.* **2002**, *41* (15), 3983–3989. (e) Ackermann, J.; Meyer, F.; Kaifer, E.; Pritzkow, H. *Chem.—Eur. J.* **2002**, *8* (1), 247–258. (f) Neves, A.; Rossi, L. M.; Bortoluzzi, A. J.; Szpoganicz, B.; Wiezbicki, C.; Schwingel, E.; Haase, W.; Ostrovsky, S. *Inorg. Chem.* **2002**, *41* (7), 1788–1794. (g) Monzani, E.; Quinti, L.; Perotti, A.; Casella, L.; Gullotti, M.; Randaccio, L.; Geremia, S.; Nardin, G.; Faleschini, P.; Tabbi, G. *Inorg. Chem.* **1998**, *37* (5), 553–562. (h) Granata, A.; Monzani, E.; Casella, L. *J. Biol. Inorg. Chem.* **2004**, *9*, 903–913. (i) Selmeczi, K.; Réglier, M.; Giorgi, M.; Speier, G. *Coord. Chem. Rev.* **2003**, *245* (1–2), 191–201. (j) Selmeczi, K.; Réglier, M.; Speier, G.; Peintler, G. *React. Kinet. Catal. Lett.* **2004**, *81* (1), 143–151. (k) Chen, P.; Solomon, E. I. *Proc. Natl. Acad. Sci. U.S.A.* **2004**, *101* (36), 13105–13110. (l) Siegbahn, P. E. M. *J. Biol. Inorg. Chem.* **2004**, *9* (5), 577–590. (m) Koval, I. A.; Huisman, M.; Stassen, A. F.; Gamez, P.; Roubeau, O.; Belle, C.; Pierre, J. L.; Saint-Aman, E.; Luken, M.; Krebs, B.; Lutz, M.; Spek, A. L.; Reedijk, J. *Eur. J. Inorg. Chem.* **2004**, 4036–4045.

(7) (a) Simándi, T. L.; Simándi, L. I. *J. Chem. Soc., Dalton Trans.* **1999**, *24*, 4529–4533. (b) May, Z.; Besenyei, G.; Simándi, L. I.; Asari, D.; Funabiki, T. *J. Inorg. Biochem.* **2001**, *86* (1), 332–332. (c) Simándi, L. I.; Simándi, T. M.; May, Z.; Besenyei, G. *Coord. Chem. Rev.* **2003**, *245* (1–2), 85–93. (d) Simándi, T. M.; May, Z.; Szigyártó, I. C.; Simándi, L. I. *Dalton Trans.* **2005**, 365–368.

(8) (a) Krebs, B.; Pursche, D.; Rompel, A.; Triller, M. U.; Hsieh, W. Y.; Pecoraro, V. L. *J. Inorg. Biochem.* **2003**, *96* (1), 172–172. (b) Triller, M. U.; Pursche, D.; Hsieh, W. Y.; Pecoraro, V. L.; Rompel, A.; Krebs, B. *Inorg. Chem.* **2003**, *42* (20), 6274–6283. (c) Paine, T. K.; Weyhermüller, T.; Bothe, E.; Wieghardt, K.; Chaudhuri, P. *Dalton Trans.* **2003**, 3136–3144. (d) Mukherjee, S.; Weyhermüller, T.; Bothe, E.; Wieghardt, K.; Chaudhuri, P. *Dalton Trans.* **2004**, 3842–3853.

(9) (a) Simándi, L. I.; Barna, T. M.; Argay, Gy.; Simándi, T. L. *Inorg. Chem.* **1995**, *34* (25), 6337–6340. (b) Simándi, L. I.; Simándi, T. L. *J. Chem. Soc., Dalton Trans.* **1998**, *19*, 3275–3280. (c) Simándi, L. I. In *Advances in Catalytic Activation of Dioxygen by Metal Complexes*; Simándi, L. I., Ed.; Kluwer Academic Publishers: Dordrecht, The Netherlands, 2003; pp 265–328.

(10) (a) Simándi, L. I. *Catalytic Activation of Dioxygen by Metal Complexes*; Kluwer Academic Publishers: Dordrecht, The Netherlands, 1992; p 396.

(11) Simándi, L. I. *Advances in Catalytic Activation of Dioxygen by Metal Complexes*; Kluwer Academic Publishers: Dordrecht, The Netherlands, 2003.

(12) (a) Jones, R. D.; Summerville, D. A.; Basolo, F. *J. Am. Chem. Soc.* **1978**, *100* (14), 4416–4424. (b) Valentine, J. S.; Quinn, A. E. *Inorg. Chem.* **1976**, *15* (8), 1997–1999.

(13) Bhula, R.; Gainsford, G. J.; Weatherburn, D. C. *J. Am. Chem. Soc.* **1988**, *110* (22), 7550–7552.

(14) Bossek, U.; Weyhermüller, T.; Wieghardt, K.; Nuber, B. J.; Weiss, J. *J. Am. Chem. Soc.* **1990**, *112* (17), 6387–6388.

(15) Lever, A. B. P.; Wilshire, J. P.; Quan, S. K. *J. Am. Chem. Soc.* **1979**, *101* (13), 3668–3669.

(16) Chin, D. H.; Sawyer, D. T.; Schaefer, W. P.; Simmons, C. J. *Inorg. Chem.* **1983**, *22* (5), 752–758.

(17) Barratt, D. S.; Gott, G. A.; McAuliffe, C. A. *J. Chem. Soc., Dalton Trans.* **1988**, *8*, 2065–2070.

(18) (a) Kitajima, N.; Komatsuzaki, H.; Hikichi, S.; Osawa, M.; Moro-oka, Y. *J. Am. Chem. Soc.* **1994**, *116* (25), 11596–11597. (b) Kitajima, N.; Singh, U. P.; Amagai, H.; Osawa, M.; Moro-oka, Y. *J. Am. Chem. Soc.* **1991**, *113* (20), 7757–7758.

(19) Frederick, F. C.; Taylor, L. T. *Polyhedron* **1986**, *5* (3), 887–893.

(20) Horwitz, C. P.; Winslow, P. J.; Worden, J. T.; Lisek, C. A. *Inorg. Chem.* **1993**, *32* (1), 82–86.

(21) Coleman, W. M.; Taylor, L. T. *Inorg. Chim. Acta* **1978**, *30*, L291–L293.

(22) (a) Dismukes, G. C.; Sheats, J. E.; Smegal, J. A. *J. Am. Chem. Soc.* **1987**, *109* (23), 7202–7203.

(23) Perrée-Fauvet, M.; Gaudemer, A.; Bonvoisin, J.; Girerd, J. J.; Boucly-Goester, C.; Boucly, P. *Inorg. Chem.* **1989**, *28* (23), 3533–3538.

(24) Fábián, I.; Csordás, V. In *Advances in Inorganic Chemistry*; Van Eldik, R., Hubbard, C. D., Eds.; Academic Press: Amsterdam, The Netherlands, 2003; Vol. 54, Issue 5, pp 395–461.

(25) Hitomi, Y.; Ando, A.; Matsui, H.; Ito, T.; Tanaka, T.; Ogo, S.; Funabiki, T. *Inorg. Chem.* **2005**, *44*, 3473–3478.

(26) Singh, S.; Chakravortty, V.; Dash, K. C. *Indian J. Chem., Sect. A: Inorg., Phys., Theor. Anal.* **1989**, *28* (3), 255–257.

the experiments. Spectra were accumulated over the initial 30 min of the reaction.

Electrospray ionization mass spectrometry (ESI-MS) experiments were performed on a PE-SCIEX API 2000 triple-quadrupole mass spectrometer. Spectra were acquired in positive mode with a 4800-V spray voltage and a 30-V orifice voltage; the source housing was kept at room temperature. Samples were dissolved in MeOH. The instrument was used in Q_1 scan mode in the range of m/z 50−1000.

The oxidation was followed by (i) recording the time evolution of UV/vis spectra on a Hewlett-Packard 8453 diode-array spectrophotometer and (ii) measuring the volume of O_2 absorbed.

The rates of O_2 uptake were measured in a constant-pressure gas-volumetric apparatus, described earlier.[8a] The reaction was started by dropping the solid Mn^{II} catalyst **1** precursor into a vigorously stirred, thermally equilibrated MeOH solution of H_2-dtbc from a sample holder manipulated from the outside. The rate of O_2 absorption was independent of the stirring rate, excluding eventual diffusion control effects.

Throughout this paper, M = mol dm^{-3}.

[Mn₂(HL)₂][B(C₆H₅)₄]₂ (1) was prepared by dissolving H_2L (538 mg, 2 mmol) and $MnCl_2·4H_2O$ (198 mg, 1 mmol) in MeOH at 25 °C. The resulting red solution was stirred for 30 min. After the addition of $NaB(C_6H_5)_4$ (342 mg, 1 mmol) in 5 mL of MeOH, an orange precipitate formed, which was collected by filtration and dried at ambient temperature. The complex was recrystallized from MeOH/CH_2Cl_2 (1:1) to give red single crystals suitable for analysis by X-ray diffraction. Yield: 55%. Anal. Calcd for [Mn-$(C_{12}H_{22}N_5O_2)]_2[B(C_6H_5)_4]_2$: C, 67.30; H, 6.59; N, 10.90. Found: C, 67.01; H, 6.64; N, 10.92. IR (KBr disk): $ν$ 3441(m), 3058(m), 1645(m), 1424(m), 1054(s), 735(s), 711(s), 612(m) cm^{-1}.

Crystal Structure Determination of Complex 1. Crystal data:[27−30] $C_{36}H_{42}BMnN_5O_2$, $M = 642.50$, monoclinic, $a = 14.143(1)$ Å, $b = 14.226(2)$ Å, $c = 17.800(2)$ Å, $U = 3308.2(6)$ Å^3, space group $P2_1/c$, $Z = 4$, $μ = 3.552$ mm^{-1}, 4849 reflections measured, 4551 unique [R(int) =0.0297], which were used in all calculations. Final R indices [$I > 2σ(I)$] were R1 = 0.0569 and wR2 = 0.1122. The C3 atom splits into two positions in a 0.81:0.19 ratio.

Results and Discussion

X-ray Structure of 1. The molecular structure of the dimeric catalyst precursor **1** is shown in Figure 1 (the two BPh_4^- ions are omitted for clarity). Each monomeric unit contains one HL^- ligand, having one oximato(1−) and one oxime group. The coordination spheres of both Mn atoms (that of Mn1 shown in Figure 2) are strongly distorted octahedra with four N atoms (N1−N4) in the quasi-equatorial plane and the N5 atom in the pseudoaxial position. The other axial position is occupied by a bridging oximato O atom from the other monomeric unit. The result is a bis($μ$-oximato-$1κN:2κO$) dimer formed around the inversion center. There is intramolecular H bonding between the oxime H atoms and the O atoms of the oximato moiety [O1−H1o···O2: H−O 0.71 Å, H···O 1.98 Å, O···O 2.568(6) Å, <(O−H···O) 141-

(27) North, A. C. T.; Philips, D. C.; Mathews, F. S. *Acta Crystallogr.* **1968**, *A24*, 351−359.

(28) Sheldrick, G. M. *SHELXS-97, Program for Crystal Structure Solution*; University of Göttingen: Göttingen, Germany, 1997.

(29) *International Tables for X-ray Crystallography*; Wilson, A. J. C., Ed.; Kluwer Academic Publishers: Dordrecht, The Netherlands, 1992; Vol. C; Tables 6.1.1.4 (pp 500−502), 4.2.6.8 (pp 219−222), and 4.2.4.2 (pp 193−199).
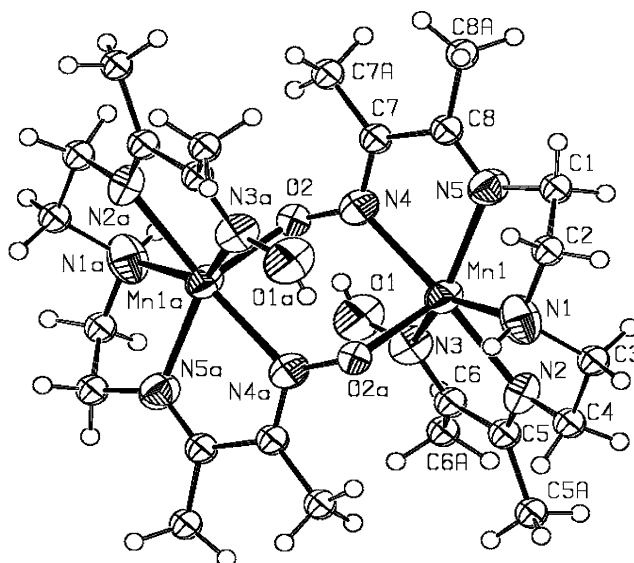
Figure 1. Molecular diagram[29] of the dication of **1**, $[Mn_2(HL)_2]^{2+}$, with the numbering of atoms. The minor disorder component [C(3×), H(3 × 1), H(3 × 2), and H(1×)] is omitted for clarity. Atomic displacement parameters are represented at the 50% probability level.

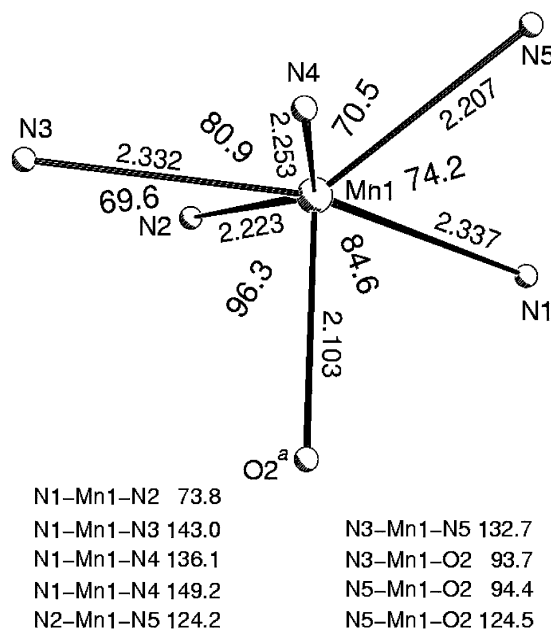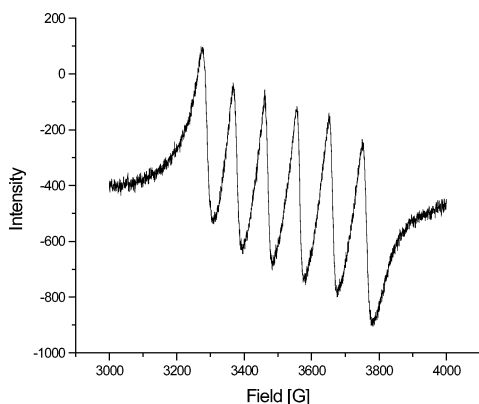| N1−Mn1−N2	73.8		
N1−Mn1−N3	143.0	N3−Mn1−N5	132.7
N1−Mn1−N4	136.1	N3−Mn1−O2	93.7
N1−Mn1−N4	149.2	N5−Mn1−O2	94.4
N2−Mn1−N5	124.2	N5−Mn1−O2	124.5

Figure 2. Coordination sphere of Mn1 with distances (Å) and angles (deg).

(8)°] and a rather weak H bond between the same donor and the N4 of the same ligand [O1−H1o···N4: H−O 0.71 Å, H···N 2.62 Å, O···N 3.062(7), O−H···N 123(8)°], conferring additional stability on the dimer.

ESI-MS. For ESI-MS, the dimeric Mn^{II} complex **1** was dissolved in MeOH and measured in positive ion mode. In the spectra, an intensive singly charged ion was observed, corresponding to the 5-coordinate monomeric $[Mn^{II}(HL)]^+$ structure ($m/z = 323.2$). Besides this, the 6-coordinate methanolato complex $[Mn^{II}(HL)(CH_3OH)]^+$ ($m/z = 355$) could also be observed in medium intensity. The free protonated ligand $[H_2L + H^+]$ ($m/z = 270.1$) was detected in low intensity only. These results strongly indicate that the predominant species in MeOH should be $[Mn^{II}(HL)(CH_3-$

Figure 3. Dissociation of dimer **1** into monomeric units **2**: ESR spectrum of a 2.0×10^{-3} M solution of **1** in MeOH immediately after dissolution at room temperature ($g = 2.007$, coupling constant = 96.4 G).
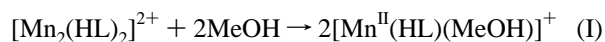
Scheme 1. NaOH-Catalyzed Oxidation of H$_2$dtbc
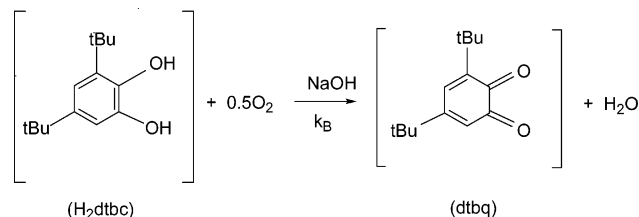
Scheme 2. Base-Catalyzed Equilibrium Binding of O$_2$, Leading to a Peroxy Intermediate
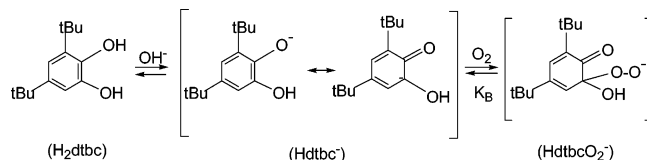
OH)]$^+$, a large percentage of which loses coordinated CH$_3$-OH upon evaporation, generating the $m/z = 323.2$ species.

ESR Spectroscopy. The ESR spectra in a MeOH solution also provide information upon the nature of Mn species present. The solid dimer **1** dissolved in acetonitrile is ESR-silent. However, immediately upon dissolution of complex **1** in MeOH at room temperature, the typical six-line pattern of monomeric Mn^{II} appears (Figure 3) and persists for several hours, indicating that **1** dissociates into monomeric units **2** (eq I), which are stabilized by coordination of MeOH as the sixth ligand. Because the intensity of the ESR spectrum does not change in time, the dissociation can be regarded as complete. Dissociation does not take place in acetonitrile.

$$[\text{Mn}_2(\text{HL})_2]^{2+} + 2\text{MeOH} \rightarrow 2[\text{Mn}^{II}(\text{HL})(\text{MeOH})]^+ \quad (\text{I})$$

Base-Catalyzed Oxidation of H$_2$dtbc. The base-catalyzed oxidation of H$_2$dtbc to 3,5-di-*tert*-butyl-1,2-benzoquinone (dtbq) by O$_2$ is known to take place in the presence of dilute (<0.06 M) NaOH in MeOH at room temperature[31] (Scheme 1).

The reactive species in this process is the catecholato monoanion, Hdtbc$^-$, which can be generated by the known
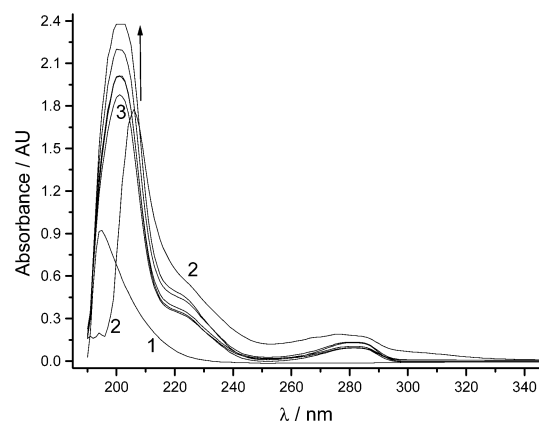
(30) Spek, A. L. *Acta Crystallogr.* **1990**, *A46*, C-34 (Table A. Crystal data and structure refinement).
(31) Grinstead, R. R. *Biochemistry* **1964**, *3*, 1308−1314.

Figure 4. Spectra of components (1, TEA; 2, H$_2$dtbc) and evolution of spectra for base-catalyzed oxidation (3). 1: [TEA]$_0$ = 3.86×10^{-3} M; l = 1 mm; T = 25 °C. 2: [H$_2$dtbc]$_0$ = 3.8×10^{-5} M; l = 1 cm; T = 25 °C. 3: [H$_2$dtbc]$_0$ = 3.92×10^{-4} M + [TEA]$_0$ = 3.74×10^{-4} M; l = 1 mm; T = 25 °C. t = 0−1020 s.
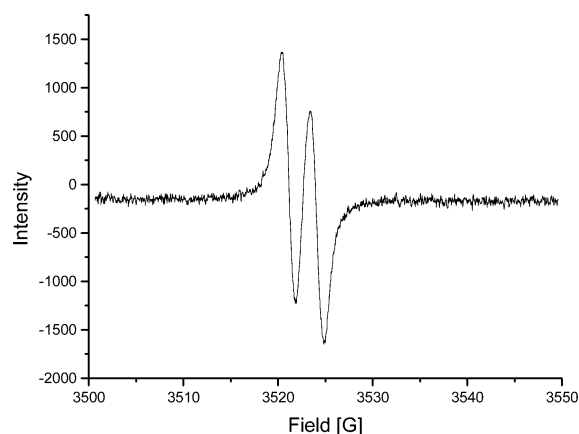

Figure 5. ESR spectrum of the semiquinone intermediate.

reaction of H$_2$dtbc with a hydroxide ion. It binds O$_2$ at room temperature, affording the hydroperoxo adduct HdtbcO$_2^-$ (Scheme 2).[31]

Deprotonation of H$_2$dtbc can also be effected by N bases of suitable strength, an approach we used in this work. Figure 4 shows the spectral changes (3) observed during TEA-catalyzed oxidation of H$_2$dtbc together with the spectra of H$_2$dtbc (2) and TEA itself (1). The series of spectra (3) corresponds to rapid deprotonation of H$_2$dtbc by TEA to Hdtbc$^-$, followed by oxidation to dtbq. The simultaneous increase of the bands at 203, 282, and 404 nm and of the shoulder at 220 nm, as well as the lack of isosbestic points, indicates the absence of absorbing products other than dtbq.

An important feature of the base-catalyzed oxidation is the appearance of the 3,5-di-*tert*-butyl-1,2-benzosemiquinon-ate(1−) anion radical (dbsq$^{\bullet-}$) as an intermediate detectable by ESR spectroscopy (Figure 5). No detection is possible spectrophotometrically because of its low concentration reached during the oxidation (the sodium salt of dbsq$^{\bullet-}$ has λ_{max} = 730 nm and ϵ_{730} = 680 M^{-1} cm^{-1}).[32] This should be taken into account by the proposed reaction mechanism.

When other N bases are used as catalysts, the rate varies as a function of the base strength. Some examples are shown

(32) White, L. S.; Hellman, E. J.; Que, L., Jr. *J. Org. Chem.* **1982**, *47*, 3766−3769.

Table 1. Initial Rate of H_2dbc Oxidation Catalyzed by N Bases of Different Strength (Solvent MeOH, $[H_2Dtbc]_0 = 3.86 \times 10^{-3}$ M, $[Base]_0 = 3.86 \times 10^{-3}$ M, under Air)

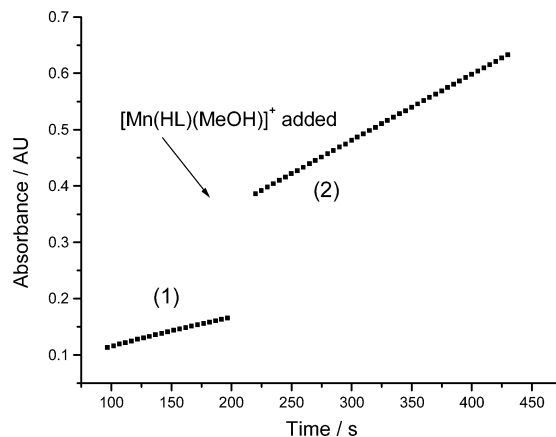| base	pK_a	initial rate/M s^{-1}
none	na	1.68×10^{-9}
pyridine	5.33[33a]	1.83×10^{-9}
1-methylimidazole	7.06[33a]	3.79×10^{-9}
triethylamine	9.73[33a]	4.34×10^{-7}
1,8-bis(dimethylamino)naphthalene (proton sponge)	12.34[33b]	3.41×10^{-7}

in Table 1, indicating that the rate of base-catalyzed oxidation depends on the pK of the added N base. This is in line with the generalized Scheme 2, where deprotonation of H_2dtbc takes place by the added base, generating the monoanion Hdtbc$^-$, which is the reactive intermediate toward O_2. In the presence of a proton sponge, the rate does not increase further, indicating that the dianion has about the same reactivity as Hdtbc$^-$.

Individual volumetric O_2 absorption curves show the saturation behavior leveling off at the stoichiometric amount corresponding to Scheme 1, i.e., upon reduction of both O atoms to H_2O. The reaction can be restarted by repeated addition of H_2dbc to mixtures in which the O_2 uptake has already ceased. For further work, we have selected TEA to ensure significant deprotonation to the monoanion.

Effect of Added [Mn^{II}(HL)(MeOH)]$^+$ on the Oxidation of H_2dtbc. When present alone in MeOH, the complex [Mn^{II}-(HL)(MeOH)]$^+$ does not react with O_2 nor does it catalyze catechol oxidation. However, when added to a solution in which the TEA-catalyzed oxidation of H_2dtbc is in progress, it brings about a remarkable increase (ca. 2.5-fold) in the oxidation rate. This acceleration is illustrated by the absorbance at 404 nm displayed in Figure 6 as a function of time. The corresponding two series of spectra are given in the Supporting Information as Figures 1S and 2S. Series 1 refers to the TEA-catalyzed oxidation, whereas series 2 was recorded after the addition of 5.2×10^{-4} M [Mn^{II}(HL)-(MeOH)]$^+$ in MeOH to the reacting solution.

Upon the addition of MnCl$_2$ instead of [Mn^{II}(HL)-(MeOH)]$^+$ to the reacting solution, a dark-brown solution formed, but its spectra did not show the formation of dtbq. Instead, MnO$_2$ gradually precipitated, indicating oxidation to Mn^{III} followed by disproportionation.

In another experiment, complex **1** was dissolved in O_2-saturated MeOH, containing H_2dtbc. According to ESR spectroscopy of this solution, the six-line pattern of monomeric [Mn^{II}(HL)(MeOH)]$^+$ appeared, but no oxidation of H_2-dtbc (O_2 absorption) took place. However, upon the addition of TEA, the oxidation of H_2dtbc started immediately as shown by (a) the absorption of O_2, (b) development of a strong absorption band centered at 404 nm, and (c) the appearance of the characteristic ESR spectrum of dbsq$^{\bullet-}$, which is a narrow doublet at $g = 2.0032$ (Figure 5)[34]

(33) (a) Stability *Constants of Metal-ion Complexes*; Compiled by A. E. Martell; Special Publication No. 17, Section II, Organic Ligands; The Chemical Society: London, 1964; p 489. (b) Brzezinski, B.; Grech, E.; Malarski, Z.; Sobczyk, L. *J. Chem. Soc., Perkin Trans. 2* **1991**, *6*, 857−859.
(34) Buchanan, R. M.; Fitzgerald, B. J.; Pierpont, C. G. *Inorg. Chem.* **1979**, *18* (12), 3439−3444.

Figure 6. Rate of the base-catalyzed oxidation (section 1) and its increase upon the addition of [Mn(HL)(MeOH)]$^+$ (section 2). Rate measured spectrophotometrically by monitoring the increase of absorbance at 404 nm (1-cm cell). 1: $[H_2dtbc]_0 = 3.9 \times 10^{-3}$ M, $[TEA]_0 = 3.8 \times 10^{-3}$ M; $T = 25$ °C. 2: same as 1 but with $[Mn]_0 = 5.2 \times 10^{-4}$ M added.

superimposed on the six-line signal of [Mn^{II}(HL)(MeOH)]$^+$, persisting throughout the catalytic oxidation.

According to these results, [Mn^{II}(HL)(MeOH)]$^+$ alone does not activate O_2; however, as demonstrated by rate measurements, it accelerates the TEA-catalyzed oxidation of H_2dtbc when added to a reacting mixture. This points to a novel oxidation path via an intermediate formed from HdtbcO$_2^-$ and [Mn^{II}(HL)(MeOH)]$^+$, producing an acceleration relative to the base-catalyzed oxidation. This path can be termed Mn-enhanced base catalysis. As expected, formation of the dbsq$^{\bullet-}$ intermediate can also be detected in the Mn-enhanced reaction.

To our knowledge, this feature has not been reported for other catechol oxidations in MeOH, where the base-catalyzed and metal-complex-catalyzed reactions run in parallel.

To elucidate the features of the combined oxidation path, the time evolution of the UV/vis spectra has been monitored spectrophotometrically (see the Supporting Information, Figure 2S).

We followed the reaction in Scheme 1 by two techniques, viz., (i) spectrophotometrically, and (ii) by measurement of the volume of O_2 absorbed by the solution.

Kinetic Measurements. O_2 absorption curves were recorded as a function of time in MeOH as the solvent. From these curves, the initial rates (V_{in}) of O_2 uptake were determined as a function of the catalyst, substrate, and TEA concentration as well as the O_2 partial pressure. The primary results are shown in the Supporting Information (Tables 1S−4S); each value shown is the average of three individual runs reproducible to within ±4%. At a constant concentration of H_2dtbc and TEA and constant O_2 pressure (O_2 concentration), the initial rate was found to be proportional to the catalyst concentration (Figure 7). A clean first-order behavior was found when varying the concentration of O_2 (Figure 8). Saturation-type curves were observed upon varying the H_2-dtbc concentration at constant catalyst, TEA, and O_2 concentration (Figure 9). Variation of V_{in} as a function of the TEA concentration also yielded a saturation curve (Figure 10).
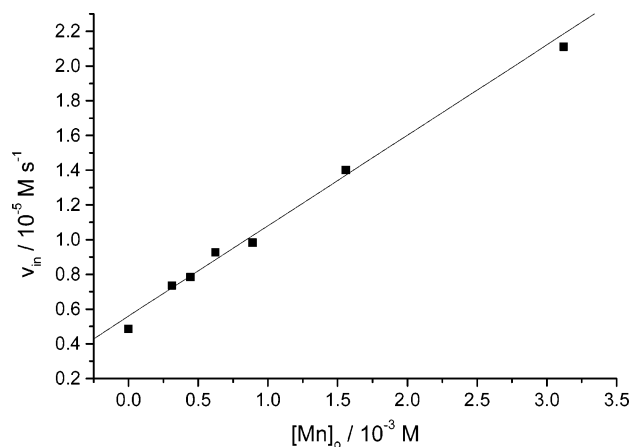
Figure 7. Plot of the initial rate against the initial concentration of the monomeric catalyst Mn (=2[**1**]). Conditions: $[H_2dtbc]_0 = 31.2 \times 10^{-3}$ M; $[TEA]_0 = 11.5 \times 10^{-3}$ M; $[O_2]_0 = 1.1 \times 10^{-3}$ M; solvent MeOH; $T = 25$ °C.
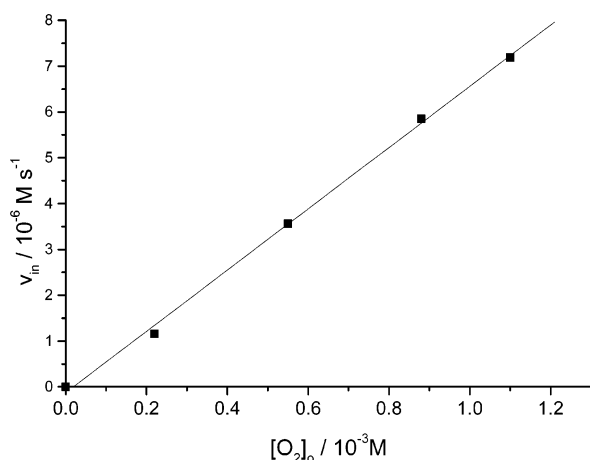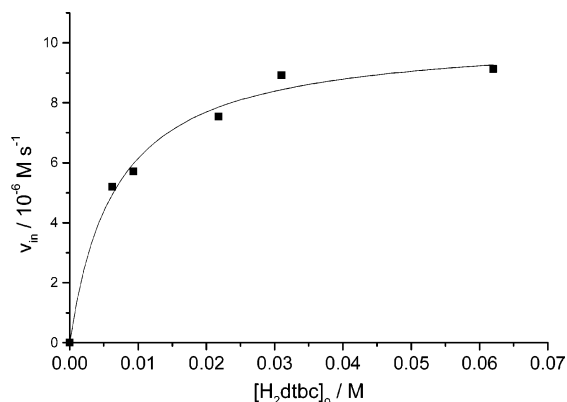

Figure 8. Dependence of the initial rate of O_2 absorption on the O_2 concentration. Conditions: $[Mn]_0 = 6.26 \times 10^{-4}$ M; $[H_2dtbc]_0 = 12.5 \times 10^{-3}$ M; $[TEA]_0 = 12.9 \times 10^{-3}$ M; solvent MeOH; $T = 25$ °C.

Figure 9. Dependence of the initial rate of O_2 absorption on the substrate concentration. Conditions: $[Mn]_0 = 6.26 \times 10^{-4}$ M; $[O_2]_0 = 1.1 \times 10^{-3}$ M; $[TEA]_0 = 11.5 \times 10^{-3}$ M; solvent MeOH; $T = 25$ °C.

The kinetic dependences shown in Figures 7−10 can be described by the empirical rate equation (II), where A, B, and C are constants.

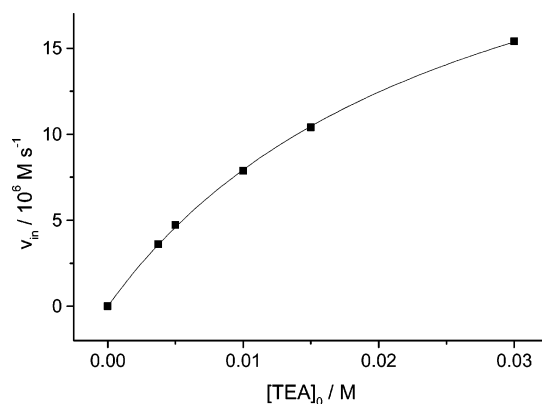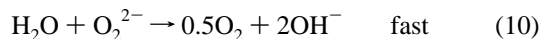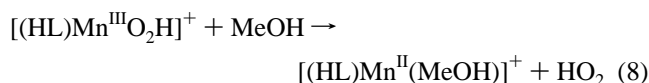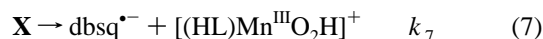$$V_{in} = \frac{\{A + B[Mn]_0\}[O_2]_0[H_2dtbc]_0}{1 + C[H_2dtbc]_0/[TEA]_0} \quad (II)$$
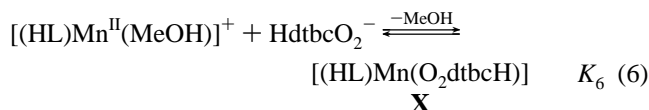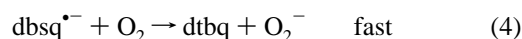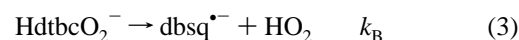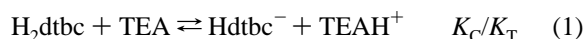
Figure 10. Dependence of the initial rate of O_2 absorption on the TEA concentration. Conditions: $[Mn]_0 = 1.0 \times 10^{-3}$ M; $[H_2dtbc]_0 = 15.0 \times 10^{-3}$ M; $[O_2]_0 = 1.10 \times 10^{-3}$ M; solvent MeOH; $T = 25$ °C.

Empirical rate law (II) is consistent with the following reaction mechanism:

$$H_2dtbc + TEA \rightleftharpoons Hdtbc^- + TEAH^+ \qquad K_C/K_T \quad (1)$$

$$Hdtbc^- + O_2 \rightleftharpoons HdtbcO_2^- \qquad K_B \quad (2)$$

$$HdtbcO_2^- \rightarrow dbsq^{\bullet-} + HO_2 \qquad k_B \quad (3)$$

$$dbsq^{\bullet-} + O_2 \rightarrow dtbq + O_2^- \qquad fast \quad (4)$$

$$HO_2 + TEA \rightleftharpoons O_2^- + TEAH^+ \qquad fast \quad (5)$$

$$[(HL)Mn^{II}(MeOH)]^+ + HdtbcO_2^- \underset{\xrightarrow{}}{\overset{-MeOH}{\rightleftharpoons}}$$
$$[(HL)Mn(O_2dtbcH)] \qquad K_6 \quad (6)$$
$$\mathbf{X}$$

$$\mathbf{X} \rightarrow dbsq^{\bullet-} + [(HL)Mn^{III}O_2H]^+ \qquad k_7 \quad (7)$$

$$[(HL)Mn^{III}O_2H]^+ + MeOH \rightarrow$$
$$[(HL)Mn^{II}(MeOH)]^+ + HO_2 \quad (8)$$

$$2O_2^- \rightarrow O_2 + O_2^{2-} \qquad fast \quad (9)$$

$$H_2O + O_2^{2-} \rightarrow 0.5O_2 + 2OH^- \qquad fast \quad (10)$$

According to the proposed mechanism (1)−(10), the oxidation of H_2dtbc in the presence of TEA takes place via deprotonation to the monoanion (1) followed by the formation of the O_2 adduct $HdtbcO_2^-$ in step 2 (for the structure of this hydroperoxide, see Scheme 2). It decomposes in rate-limiting step 3 to HO_2 (stabilized as O_2^-) and the semi-quinonato anion radical $dbsq^{\bullet-}$, which is rapidly oxidized to the product $dtbq$ by O_2 (step 4). At this point interference by $[(HL)Mn^{II}(MeOH)]^+$ becomes operative via displacement of coordinated MeOH by $HdtbcO_2^-$ in step 6, leading to the formation of $[(HL)Mn(O_2dtbcH)]^+$ (**X**). Rapid elimination of $dbsq^{\bullet-}$ in step 7 and of HO_2 in step 8 (with immediate deprotonation to O_2^-) regenerates $[(HL)Mn^{II}(MeOH)]^+$ and

Table 2. Summary of the Rate and Equilibrium Constants (MeOH, 25 °C)

source	$C = K_C/K_T$	$B = k_6K_5K_B/M^{-2} s^{-1}$	$A = k_B/M^{-1} s^{-1}$	slope/s^{-1}
substrate dep. (Figure 11)	1.72 ± 0.05	895 ± 27	0.84 ± 0.025	na
[TEA] dep. (Figure 12)	1.75 ± 0.05			na
O_2-dep. (exp) (Figure 10)	na	na	na	$(6.69 \pm 0.33) \times 10^{-3}$
O_2-dep. (calcd) (Figure 10)	na	na	na	$(6.53 \pm 0.31) \times 10^{-3}$
[Mn]$_0$ dep. (exp) (Figure 9)	na	na	na	$(5.25 \pm 0.16) \times 10^{-3}$
[Mn]$_0$ dep. (calcd) (Figure 9)	na	na	na	$(5.39 \pm 0.14) \times 10^{-3}$

closes the Mn-enhanced cycle. The dbsq$^{•-}$ released is rapidly oxidized to dtbq by O_2 in step 4.[35a]

While steps 1−7 account for the formation of intermediate dbsq$^{•-}$ and of the observed oxidation product (dtbq), fast steps 9 and 10 describe how intermediate O_2^- is converted to OH$^-$ (the final reduction product of O_2) via the peroxo (O_2^{2-}) oxidation state.

The kinetic equation based on the proposed mechanism can be obtained as follows.

If the initial concentration of $[(HL)Mn^{II}(MeOH)]^+$ is denoted by [Mn]$_0$, the rate of oxidation (V_{in}) can be written as

$$V_{in} = k_B[HdtbcO_2^-] + k_7K_6[Mn]_0[HdtbcO_2^-] = k_BK_B$$
$$[Hdtbc^-][O_2] + k_7K_BK_6[Hdtbc^-][O_2][Mn]_0 =$$
$$(k_B + k_7K_6[Mn]_0)K_B[Hdtbc^-][O_2] \quad (11)$$

An approximate expression for [Hdtbc$^-$] (eq 12) can be obtained from the mass balance for H_2dtbc and TEA in combination with the required protonation constants (see the Supporting Information, eqs 1S−12S).

$$[Hdtbc^-] = \frac{[H_2dtbc]_0}{1 + (K_C/K_T)[H_2dtbc]_0/[TEA]_0} \quad (12)$$

Upon substitution of eq 12 into eq 11, we obtain the kinetic equation (13).

$$V_{in} = \frac{(k_BK_B + k_7K_6K_B[Mn]_0)[O_2][H_2dtbc]_0}{1 + (K_C/K_T)[H_2dtbc]_0/[TEA]_0} \quad (13)$$

On comparison of eq 13 with the constants of empirical rate law (II), we can calculate the following kinetic and equilibrium constants:

$$A = k_BK_B = 0.84 \pm 0.025 \text{ M}^{-1} \text{ s}^{-1}$$

$$B = k_7K_6K_B = 895 \pm 27 \text{ M}^{-2} \text{ s}^{-1}$$

$$C = K_C/K_T = 1.73 \pm 0.05$$

$$B/A = k_7K_6K_B/k_BK_B = 1065 \pm 60 \text{ M}^{-1}$$

Kinetic equation (13) has the same form as the empirical rate law (II); therefore, mechanism (1)−(10) is consistent

(35) (a) Denisov, E. T. The oxidation of alcohols, ketones, ethers, esters and acids in solution. In *Liquid-Phase Oxidation, Comprehensive Chemical Kinetics*; Bamford, C. H., Tipper, C. F. H., Eds.; Elsevier: Amsterdam, The Netherlands, 1980; Vol. 16. (b) Simándi, L. I. *Catalytic Activation of Dioxygen by Metal Complexes*; Kluwer Academic Publishers: Dordrecht, The Netherlands, 1992; pp 257−259.

Scheme 3. Rate-Controlling Elimination of $[(HL)Mn^{III}(O_2H)]$ from Intermediate **X** in Step 7 of the Mn-Enhanced Path
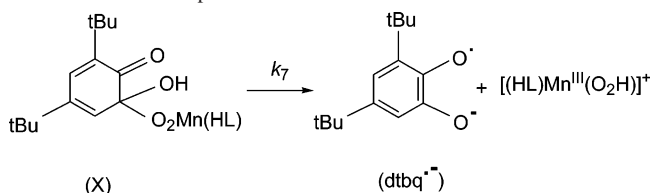
with the observed kinetic behavior. Figures 7−10 have been used to determine the parameters of eq 13. The independent parameters are k_B, $k_7K_6K_B$, and K_C/K_T. They can be determined by fitting eq 13 to the curves in both Figures 9 and 10. The results are shown in Table 2. Consistency with the catalyst and O_2 dependence (Figures 7 and 8) was demonstrated by calculating the slopes of those straight lines using the average best-fit parameters of Figures 9 and 10. The agreement is rather good, as can be seen from Table 2. The intercepts of both lines are too small to permit any reliable calculations; therefore, they were not used for showing the consistency.

Discussion

This work demonstrates that the base-catalyzed catecholase-type oxidation of H_2dtbc by O_2 is accelerated by the dioximatomanganese(II) complex, $[Mn^{II}(HL)(MeOH)]^+$, which by itself does not catalyze the catecholase reaction. There is no interaction betweeen $[Mn^{II}(HL)(MeOH)]^+$ and O_2 in the absence of base, but when the complex is added to a solution in which the TEA-catalyzed oxidation of H_2dtbc by O_2 is in progress, a distinct acceleration can be observed.

A detailed kinetic analysis of the Mn^{II}-enhanced, TEA-catalyzed reaction has shown the validity of kinetic equation (13), which is consistent with the reaction mechanism (1)−(10). It involves two reaction paths, viz., base-catalyzed and Mn-enhanced oxidation. In the base-catalyzed path, the catalyst is TEA, deprotonating H_2dtbc to the monoanion. O_2 is activated via binding to Hdtbc$^-$, generating the hydroperoxo species HdtbcO$_2^-$ (Scheme 2), which either decomposes directly to the semiquinone anion radical or, alternatively, is first bonded to $[(HL)Mn^{II}(CH_3OH)]^+$, generating the intermediate $[(HL)Mn(O_2dtbcH)]$ and only then does it yield dbsq$^{•-}$ in the rate-controlling step 7 (Scheme 3). The latter, together with step 6, is the Mn-enhanced oxidation pathway, in which the active intermediate of the base-catalyzed path is made more reactive by complexation with $[(HL)Mn^{II}(CH_3OH)]^+$. The dbsq$^{•-}$ generated via these paths is thereafter oxidized to dtbq by O_2.

An additional source of useful mechanistic information about the nature of the rate-determining step is the kinetic isotope effect (KIE). Previous examples of dioximatometal-

(II) complexes, viz., cobaloxime(II) and ferroxime(II), acting as functional catecholase and phenoxazinone synthase models[36] exhibited deuterium KIEs in the interval of 1.8−3.5, indicating a variable extent of H-atom transfer from 3,5-dtbc or 2-aminophenol hydroxy groups to coordinated O_2 in the rate-limiting step.[7d] These KIEs are close to the theoretical values,[37] corrected by equilibrium effects, for nonlinear O···H···O transition states involving the rigid, square-planar cobaloxime(II) and ferroxime(II). Lower values of ca. 1.2−1.1 were observed for Fe^{II} complexes of more flexible dioximato ligands.[7d] Significantly, the KIE of the combined base-catalyzed and Mn-enhanced catecholase reaction was found to be 1.02 even after correction for equilibrium effects.[7d]

The lack of a significant KIE indicates no direct transfer of a H atom from the aromatic OH group to the superoxo ligand in the rate-controlling step.

Work is in progress to further elucidate the mechanistic features of oxidative dehydrogenation mechanisms in biomimetic oxidations.

Supporting Information Available: Evolution of visible spectra, initial rates of O_2 uptake as a function of the catalyst, O_2, substrate, and TEA concentration, derivation of an approximate expression for [$Hdtbc^-$], and X-ray crystallographic data in CIF format. This material is available free of charge via the Internet at http://pubs.acs.org.

IC060618V

(36) Șimándi, T. M.; Simándi, L. I.; Győr, M.; Rockenbauer, A.; Gömöry, Á. *Dalton Trans.* **2004**, *7*, 1056−1060.
(37) More O'Ferrall, R. A. *J. Chem. Soc. B* **1970**, 785−790.